3 Molecular Crystal Project

Project Leader: Reiji Kumai

In this project, electronic correlation in molecular crystal systems is being investigated to elucidate novel phenomena such as superconductivity and charge ordering. We are analyzing crystal structures of molecular crystals under high pressure and/or at low temperature to elucidate the origins of phase transitions.

3-1 X-ray structural study of proton-electron coupled single-component molecular conductors

Realization of purely organic single-component molecular metals has been one of the long-standing open problems in chemistry, physics, and materials science. As is well known, purely organic materials are normally insulating. In this paper, we unveil a new type of purely organic single-component molecular conductor based on a catechol-fused ethylenedithiotetrathiafulvalene, H_2Cat-EDT-TTF, and its diselena analogue, H_2Cat-EDT-ST (Fig. 1a). [1] These conductors are unprecedented single-component systems composed of the molecular units H_3(Cat-EDT-TTF)$_2$ and H_3(Cat-EDT-ST)$_2$, with a highly symmetric intra-unit hydrogen bond (Fig. 1b). Their electrical conductivity at room temperature, $_{rt}$ = 3.5 and 19 S cm^{-1}, is significantly higher than those of previously reported purely organic single-component systems. Moreover, under physical pressures above 1.3 GPa, metallic behavior appeared in the temperature dependence of the electrical resistivity. The higher electrical conductivity observed in our systems is attributed to the hydrogen bond-promoted delocalization of charge carriers, which are generated through the partial oxidation of the H_2Cat-EDT-TTF and H_2Cat-EDT-ST molecules. [2]

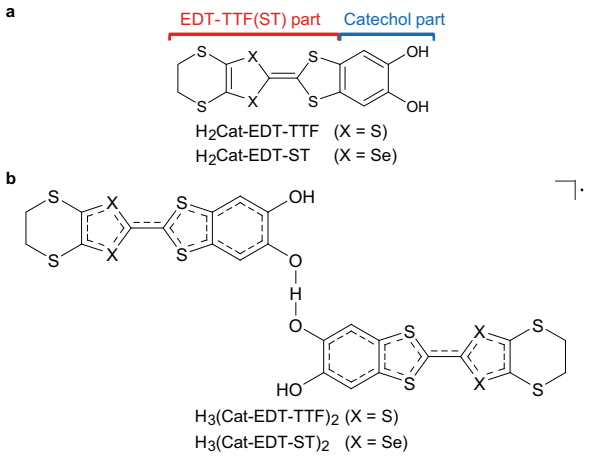

Fig. 1: Chemical structures of (a) H_2Cat-EDT-TTF (ST) and (b) molecular unit of H_3(Cat-EDT-TTF)$_2$ (ST).

A new type of purely organic single-component molecular conductor, κ-H_3(Cat-EDT-TTF)$_2$ and κ-H_3(Cat-EDTST)$_2$, hereafter referred to as κ-S and κ-Se, respectively, was obtained as black plate-like crystals by electrochemical oxidation of the corresponding donor molecules, H_2Cat-EDT-TTF and H_2Cat-EDT-ST (Fig. 1a), in the presence of the base, 2,2'-bipyridine. We emphasize here that -S and -Se are isostructural with each other, as revealed by X-ray diffraction measurements using their high-quality single crystals. Thus, the structural features of -S described below are essentially the same as those of -Se. First, we focus on the distinctive building block in a unit cell, the minimal molecular unit, shown in Figs. 1b and 2. The minimal molecular unit, the H_3(Cat-EDT-TTF)$_2$ composition, is established by the formation of an intra-unit hydrogen bond, O..H..O, between the catechol moieties of the donor molecules, where the one hydroxyl proton is deprotonated. The oxygen–oxygen distance in the hydrogen bond, d(O..O), is 2.486(5) Å and 2.509(8) Å at room temperature, and 2.453(5) Å and 2.443(8) Å at 50 K and 30 K for κ-S and κ-Se, respectively, which are much shorter than the length of the normal O–H..O type hydrogen bond, d(O..O) 2.7–3.0 Å. These short distances are evidence of the considerably high bonding energy of the hydrogen bonds for both κ-S and κ-Se. Because of this strong hydrogen bonding nature, the bonded hydrogen atom is nearly located at the center between two oxygen atoms, in contrast to the asymmetric hydrogen distribution in the normal hydrogen bonds. The bilateral Cat-EDT-TTF parts connected by the hydrogen bond are related by two-fold rotational symmetry with respect to the central hydrogen atom, namely, crystallographically equivalent with each other.

Density functional theory (DFT) calculations of this minimal molecular unit at the ROB3LYP/6-31G(d) level suggest that the HOMO of the minimal unit is spread not only on the TTF part, but also on the oxygen atoms in the catechol part, as shown in Fig. 2b. Therefore, the π electrons are widely delocalized over the whole minimal molecular unit. Next, we discuss the charge states of the minimal molecular unit. Considering the –1 valence state of the deprotonated O..H..O hydrogen bond, we can expect the +0.5 state of a TTF part to remain neutral as the whole of the minimal unit. Experimentally, the +0.5 valence state is confirmed by empirical bond-length analyses, meaning that the TTF part is partially oxidized in the construction process of the minimal molecular unit. The charge distribution is also evaluated by the electrostatic potential of the

minimal unit obtained by the UB3LYP/6-31G(d) calculations (Fig. 2c). As shown in Fig. 2c, the positive charge is extensively distributed over the EDT-TTF part, while the oxygen atoms favor negative charge, associated with the $[O..H..O]^-$ state. Thus, charge carriers are generated for κS, and probably for κ-Se as well.

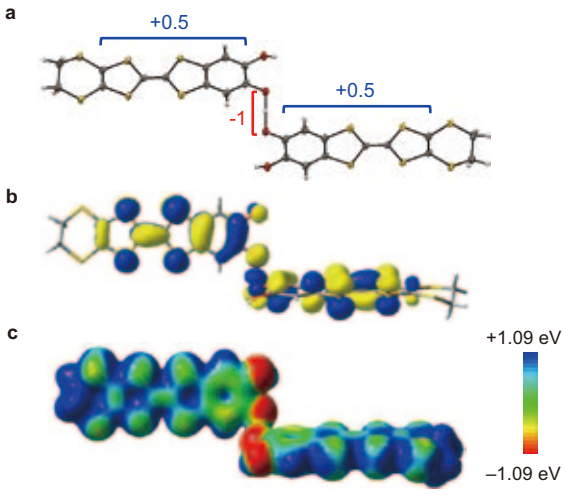

Fig. 2: (a) The molecular unit, (b) HOMO distribution calculated at the R0B3LYP/6-31G(d) level of theory, and (c) electrostatic potential surface calculated at the UB3LYP/6-31G(d) level of theory of H_3(Cat-EDT-TTF)$_2$.

The minimal molecular units are assembled into the purely organic single-component crystal, as shown in Fig. 3a. The order of the minimal unit looks like a periodic layered structure along the crystal *a*-axis. In fact, a large number of charge-transfer complexes based on TTF derivatives form the layer structure, which are usually composed of conducting electron-donor layers and insulating counter-anion layers. In our case, however, each Cat-EDT-TTF part connected by the hydrogen bond belongs to the neighboring layers, as shown in the pink and blue molecular units in Fig. 3a. These two units form a dimeric structure in a layer, which is clearly seen in the cross-sectional view perpendicular to the molecular long axis (Fig. 3b). As shown in Fig. 3b, two Cat-EDT-TTF skeletons in the pink and blue molecular units come face-to-face to form the dimeric structure. Each dimer is orthogonally arranged with the zigzag pattern, which is traditionally termed the "κ-type" molecular arrangement in the field of BEDT-TTF-based molecular conductors. In the present molecular arrangement, there exist the intra- and inter-dimer short atomic contacts of S..S 3.54 and 3.45–3.56 Å (Se..S 3.59–3.64 and 3.50–3.66 Å), respectively, for κ-S (κ-Se), as shown by the dotted lines. All of them are shorter than the sum of the van der Waals radius of sulfur and selenium atoms, that is S..S 3.60 Å and Se..S 3.70 Å, indicating that the π molecular orbitals of the minimal unit are overlapped not only within the dimer but also between the dimers. On the other hand, there exist no short intermolecular S..S or Se..S contacts along the a axis (Fig. 3a), meaning that the intermolecular interactions between the layers are considerably weaker than the intra- and inter-dimer interactions mentioned above. On the basis of this fact, assuming that the intermolecular interactions between the layers are negligible, we estimate the two-dimensional electronic band structure through the tight-binding approximation using the intra- and inter-dimer transfer integrals, b1, b2, p and q (Fig. 3b). These were obtained by the extended Hückel method calculations. The electronic band width for κ-Se is found to be larger than that for κ-S. This is because the introduction of the spatially extensive atomic orbital of selenium effectively enhances the intermolecular orbital overlap. Considering the +0.5 oxidized state of the TTF and ST parts in the minimal molecular unit, a quarter of the HOMO bands is occupied by holes, forming a hole quarter-filled band. However, the large band splitting between the upper and lower bands, comparable to the band width, provides a half-filled character for the electronic bands associated with the dimer-Mott states.

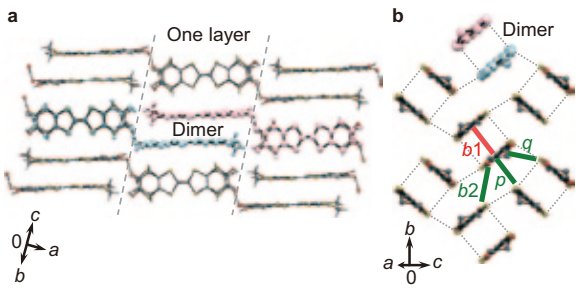

Fig. 3: (a) X-ray crystal structure, and (b) κ-type donor arrangement of κ-H_3(Cat-EDT-TTF)$_2$.

First, note that the electrical conductivity at room temperature, $_{rt} = 1/_{rt}$, is significantly high, 3.5 and 19 S cm^{-1} for κ-S and κ-Se, respectively. These values are, to the best of our knowledge, one or two orders of magnitude higher than the highest reported value, $_{rt}$ = 10^{-1} S cm^{-1}, in purely organic single-component systems. As the temperature decreases, the electrical resistivity of these systems exponentially increases, which is a typical semiconducting behavior, (T) / exp(/2k_BT), and consistent with the results of the electronic band calculations. Here, and k_B are the semiconducting energy gap and the Boltzmann constant, respectively. The energy gap / k_B, estimated by the slope of the ln vs. 1000/T plot, is 2400 K for κ-S

and 1200 K for κ-Se.

Physical pressure is a good means of changing the electronic states by modulating the intermolecular interactions. Thus, we measured the electrical conductivity under pressure for our purely organic single-component molecular conductors. It is obvious that the application of pressure reduces the slope of the ln curve, while concurrently enhancing the electrical conductivity. This result is clearly an indication of the monotonic decrease of the semiconducting energy gap with increasing pressure. Up to 1.6 GPa, however, κ-S remains semiconductive. On the other hand, we observed dramatic changes in the temperature variation in the electrical resistivity under pressure for κ-Se. The room-temperature electrical conductivity is significantly enhanced with pressure, $_{rt}$ = 180 S cm^{-1} at 2.2 GPa. This value is an order of magnitude higher than $_{rt}$ at ambient pressure. At pressures above 1.3 GPa, the electrical resistivity monotonically decreases with reducing temperature down to around 150 K, in striking contrast with the semiconducting behavior at ambient pressure, although the resistivity curve turns to increase at low temperature. Thus, metallic states emerge with the simultaneous suppression of the semiconducting energy gap by the application of pressure of only 1 GPa. To the best of our knowledge, this is the lowest metallization pressure among purely organic single-component systems. An important question is the cause of the significantly high electrical conductivity for the purely organic single-component systems κ-S and κ-Se. The hole generation by the partial oxidation of the TTF and ST parts in the minimal molecular unit resembles that in the charge-transfer complexes rather than the intrinsic half-filled electron configuration of SOMO in the neutral radicals. In the case of the normal charge-transfer complexes, the charge carriers are produced by the redox reaction between the electron donors and acceptors. In our systems, however, there exist no counter-components to accept the electrons transferred from the electron-donor molecules by oxidation. Instead, it should be noted that the [O.. H..O]$^{-}$ hydrogen bond compensates the positive charge to remain neutral as the whole of the minimal molecular unit. At the moment, the detailed process of the formation of the minimal unit and the electrochemical crystallization is unclear. Considering the analogy of the formation of phosphonic-acid and amino-acid TTFs, however, the process is possibly explained as follows. H_2Cat-EDT-TTF is diacid. In the presence of bipyridine, the monoanionic (HCat- EDT-TTF)$^{-}$ is generated. This anionic species oxidizes at a lower potential than H_2Cat-EDT-TTF itself into the zwitterionic (HCat-EDT-TTF)$^{\bullet}$. Because of the adopted choice of base, both H_2Cat-EDT-TTF and (HCat-EDT-TTF)$^{\bullet}$ are then present in solution and co-crystallize, through the symmetric hydrogen bond. As a result of the formation of the highly symmetric molecular unit, the HOMO distribution is widely extended over the whole molecular unit, as shown in Fig. 2b. The widely extended -electron molecular orbital effectively suppresses the on-site Coulomb repulsion, thus enhancing the movement of intermolecular carriers. Therefore, the construction of the molecular unit provides an itinerant character for the generated carriers. It is also important that each Cat-EDT-TTF (Cat-EDT-ST) unit of κ-S (κ-Se) is assembled into the -type molecular arrangement observed in the usual BEDT-TTF-based charge-transfer complexes, leading to the relatively strong intermolecular interactions. In fact, κ-type BEDTTTF complexes exhibit the metallic phase including superconducting states by overcoming the Mott insulating states through the control of the band width. Thus, in spite of the purely organic single-component systems, -S and -Se form a partly-filled valence band, and consequently, exhibit the highest electrical conductivity among purely organic single-component molecular conductors. In κ-Se, moreover, we found the metallic states by the application of the lowest physical pressure among purely organic single-component systems. Most studies of the molecular conductors based on hydrogen bond functionalized TTF derivatives have focused on tuning the molecular self assembly and the HOMO/LUMO energy levels. In this context, several groups have recently reported that the introduction of the hydrogen bond plays another important role, that is, the generation of charge carriers. In addition to carrier generation, our system demonstrates that the symmetric hydrogen bond constructs a new type of purely organic single-component molecular conductor which is composed of highly symmetric molecular units. Moreover, we found that the formation of the symmetric hydrogen bond promoted the intermolecular delocalization of the generated carriers, associated with the enhancement of electrical conductivity. We believe that this new type of molecular conductor with the symmetric intra-unit hydrogen bond will lead to the creation of the first purely organic single-component molecular metal at ambient pressure. A tetraselenafulvalene (TSF)-type analogue, in which all the sulfur atoms in the TTF part of the present system are replaced with selenium atoms, is a promising candidate for the ambient-pressure metal, because the intermolecular interactions are expected to be further enhanced.

References
[1] H. Kamo, A. Ueda, T. Isono, K. Takahashi, and H. Mori, Tetrahedron Lett. **53**, 4385-4388 (2012).
[2] T. Isono, H. Kamo, A. Ueda, K. Takahashi, A. Nakao, R. Kumai, H. Nakao, K. Kobayashi, Y. Murakami, and H. Mori, Nature Commun. **4**, 1344 (2013).

3-2 Above-room-temperature ferroelectricity and antiferroelectricity in benzimidazoles

Ferroelectricity, i.e. electric polarity in solids or liquid crystals that is switchable with the electric field *E*, is in increasing demand as it provides diverse entries into electronic, electromechanical, optical, and optoelectronic applications. In ferroelectrics, the spontaneous electric polarization *P* at *E* = 0 can be reversibly inverted by reversing the electric field, and the *P*–*E* curve then shows a hysteresis loop. The related antiferroelectricity phenomenon exhibits a double *P*–*E* hysteresis curve when the dipolar arrangement is reversed stepwise through the antipolar arrangement at low electric field. A very high polarization response, which is promising for capacitors, memories, and piezoelectric applications, has so far been discovered mostly in inorganic oxides containing toxic lead or rare elements such as bismuth, tantalum, niobium, and so on. The high-performance piezoelectricity of lead-based ceramics is often related to competing ferroelectric and antiferroelectric orders. To decrease our reliance on these materials and to work towards a green and sustainable society, purely organic ferroelectrics, which are expected to be used as key materials in organic, printable, and bendable electronic device applications, are being pursued as possible alternatives. Recent advances in piezoresponse force microscopy (PFM) have also revealed the nanoscale ferroelectricity of crystalline γ-form glycine and porcine aortic walls. Here we demonstrate that imidazoles carrying large electric dipoles constitute a new family of single-component ferroelectrics, as well as antiferroelectrics, in the bulk state with variable chemical substituents.

The imidazole ring is an important building block in biological systems, as exemplified by histidine, histamine, and vitamin B_{12}. In addition, these compounds are now currently utilized as ingredients in various ionic liquids as well as a corrosion inhibitor for copper. Many derivatives are commercially available, stable in air, and highly soluble in alcohols and other common organic solvents. The small imidazole molecule carries a large dipole moment (3.61 D) directed nearly parallel to the N−H bond. Imidazole can both donate and accept protons with modest acidity, and this amphoteric nature has been exploited as a guest proton-carrier in porous coordination polymers designed for anhydrous proton-conductive materials working at high temperatures. In the crystalline state, the chemical mechanism designated in Fig. 1a is anticipated for the polarization reversal. Unless the substituents allow for steric hindrance or distinct hydrogen-bonding, imidazole moieties can spontaneously assemble into a linear chain structure due to the directional nature of the intermolecular N−H…N bonds. The polarity of the chain can be inverted cooperatively by the concomitant π-bond switching and proton transfer that alters the N−H…N bond to N…H−N and vice versa. It should be noted that the scheme shown in Fig. 1a is generalized for various combinations of substituents X, Y_1, and Y_2. Therefore, the discovery of above-room-temperature ferroelectricity and antiferroelectricity we report here will stimulate systematic exploration of various structure-property relationships in the quest for lead- and rare-metal-free ferroelectric devices.

To investigate these chemical schemes, we focused first on the imidazoles of $Y_1 = Y_2$ and their ring-fused analogues, benzimidazoles (Fig. 1b), for simplicity because a number of related compounds have already been deposited in the Cambridge Structural Database. We searched the database for linear chain structures having some pseudo-symmetry to determine which candidate ferroelectrics have so far been overlooked, but we did not encounter the following example in the literature. The 5,6-dichloro-2-methylbenzimidazole (DC-MBI) crystal belongs to the orthorhombic system with the space group $Pca2_1$ (#29). The polarity of all the hydrogen-bonded chains was found to align along the crystal *c* direction (Fig. 1c). The global structure can be satisfactorily refined with slightly higher *R* factors under the higher crystal symmetry of *Pbcm* (#57) by locating a mirror symmetry plane normal to the molecular plane. In this model, the protons inevitably occupy disordered or centered locations between two nitrogen atoms.

The alternative approach is to determine the disordered or centered location of the protons. If this crystal structure represents the paraelectric state, then the protons may be ordered as asymmetric N−H…N bonds that form at temperatures lower than the Curie point and host ferroelectricity or antiferroelectricity. The other possibility is the artifacts arising from a pseudo-symmetry element assumed in the analysis misled by the global structure of minute deviation from the higher symmetry. We found that this occurs in the 2-methylbenzimidazole (MBI) crystal. The reported MBI crystal structure belongs to the tetragonal system with the symmetric space group $P4_2/n$ (#86). The protons are disordered over two sites, and their hydrogen bonds form straight bands running along either $[110]_{tetra}$

or the crystallographically equivalent $[1\bar{1}0]_{tetra}$ direction. In our analysis, the tetragonal lattice is barely lowered to the monoclinic system with the space group *Pn* (#7), which is one of the maximal subgroups of $P4_2/n$ by interchanging the crystallographic *b* and *c* axes. Because the as-grown MBI crystals are not in a single domain state but easily mix the tetragonal *a* and *b* axes, the axes and plane indices are presented here according to the tetragonal symmetry. The proton ordering is responsible for the polarity within the $(001)_{tetra}$ plane in the bulk (Fig. 1d).

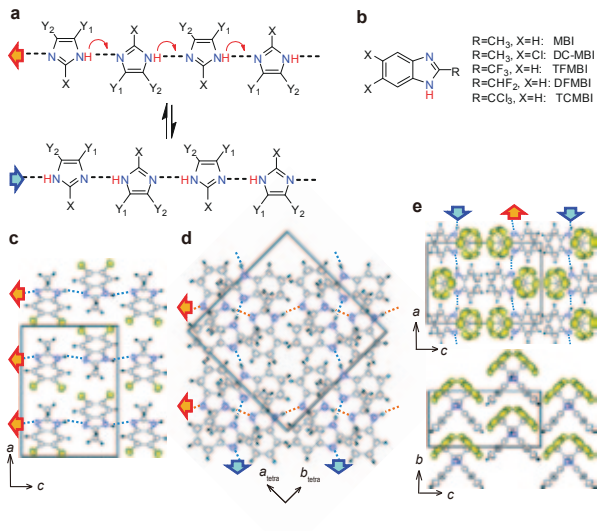

Fig. 1: Chemical and crystal structures of ferroelectric and antiferroelectric imidazoles. (a) Hydrogen bonding (broken lines) and mechanism of polarization reversal through the proton tautomerism of the imidazole moiety. (b) Chemical structures of ferroelectric and antiferroelectric benzimidazoles. (c) Crystal structure of ferroelectric DC-MBI. (d) Crystal structure of ferroelectric MBI. (e) Molecular arrangement of the antiferroelectric TCMBI.

Ferroelectric properties. We measured the *P–E* hysteresis curves for both the MBI and DC-MBI crystals with the applied electric field parallel to the hydrogen-bonded molecular sequence direction: $E||[110]_{tetra}$ for MBI and $E||[001]$ for DC-MBI. At room temperature, the MBI crystal exhibited ferroelectricity with quasi-rectangular loops and a remanent polarization as large as 5.2 μC/cm^2. The coercive field determined from the $P = 0$ intercept is 11 kV/cm at 0.2 Hz and increases with frequency. The ferroelectricity was also confirmed at higher temperatures of up to 400 K from the *P–E* hysteresis loops, which exhibited little change in the remanent polarization but did exhibit a decrease in the coercive field with temperature.

The DC-MBI crystal exhibited a coercive field at room temperature that was too high to complete a satisfactory loop even with the maximum field of 100 kV/cm. The hard switching likely reflects the elevated potential barrier for a proton to hop between the bistable potential minima due to the elongated N…N distance (2.98 Å) compared with that of MBI (2.91 Å on average). The spontaneous polarization was evaluated by reducing the coercive field at elevated temperatures. A hysteresis curve could be discerned at temperatures above 300 K. Additional contributions from electrical conduction (leakage) through the sample were suggested by the longitudinally warped *P–E* curves of the raw data but this warping could be eliminated by the double-wave method by applying a double-triangular waveform voltage. The quasi-parallelogram of the hysteresis contribution thus extracted from the data at 373 K gave a large remanent polarization of 10 μC/cm^2 and coercive field of about 60 kV/cm.

Antiferroelectric properties. The polarization was reversed at room temperature by applying an electric field parallel to the hydrogen-bonded chain for the other three imidazoles: 2-trifluoromethylbenzimidazole (TFMBI), 2-difluoromethylbenzimidazole (DFMBI), and 2-trichloromethylbenzimidazole (TCMBI) (see Fig. 1b), and their *P–E* curves, as shown in Fig. 2, are similar. At low electric fields, the polarization increases linearly with *E*, whereas quasi-step-like changes appear at higher fields with hysteresis. This double hysteresis loop is characteristic of antiferroelectricity, which appears when the free energy of an antipolar arrangement of dipolar chains is comparable to that of a polar arrangement. By subtracting the normal dielectric (linear *P–E*) component, we obtained electrically induced polarizations of about 8, 6, and 8 μC/cm^2 for TFMBI, DFMBI, and TCMBI, respectively. Such large polarizations are comparable to the remanent polarization of DC-MBI, signaling the fully aligned polarity of the dipolar chains under an electric field beyond the critical field.

According to our crystal structural analysis, these antiferroelectrics have similar molecular and hydrogen-bonded chain structures. It should be noted that the large thermal ellipsoid over two sites for each halogen atom corresponds to the rotational disorder of the trihalomethyl groups in the TFMBI and TCMBI crystals. By ignoring the proton locations, these antiferroelectric molecules have pseudo-mirror symmetry normal to the molecular plane. In reality, both the molecular and crystal symmetries are lowered by the proton ordering. The three-dimensional molecular arrangements of these crystals are not isomorphous to one another. While ferroelectricity requires a polar crystal structure, antiferroelectricity is usually related to the nonpolar structure at $E = 0$, which is true for the

TFMBI and DFMBI crystals, as they exhibit an antipolar arrangement of dipolar chains. Due to the proton ordering, the pseudo-orthorhombic lattice with the space group *Pbcm* (#57) of the TFMBI and DFMBI crystals is lowered to the monoclinic lattice with the symmetric space group $P2_1/c$ (#14). In contrast, antiferroelectric TCMBI is a polar crystal (Fig. 1e); the pseudo-orthorhombic symmetry of the polar space group $Pmc2_1$ (#26) is lowered to that of the $P2_1$ (#4) monoclinic lattice. The dipole moment component along the transverse molecular axes is arranged in an antiparallel manner, causing antiferroelectricity along the crystal *a*-axis, whereas that along the longitudinal axes cannot be cancelled out by the crystal symmetry and permanent polarity is retained along the *b*-direction normal to the hydrogen-bonded chains.

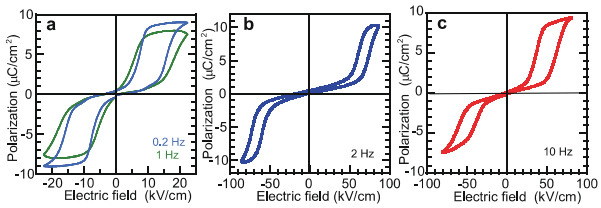

Fig. 2: Antiferroelectric properties at room temperature. The applied electric field was parallel to the direction of the hydrogen-bonded molecular sequence. (a) TFMBI, (b) DFMBI, and (c) TCMBI crystals. Molecule abbreviations are given in Fig. 1b.

Thermal properties. For all five compounds, the temperature-dependent permittivity measured along the dipolar chains simply increases with temperature at least up to ~360–380 K without any peak anomaly indicative of the Curie point. Thus, the ferroelectric or antiferroelectric phase persists from room temperature to far above room temperature. These compounds, except DC-MBI, did not display any phase transitions in differential scanning calorimetry (DSC) measurements until the samples gradually started to sublime at around 400–420 K. For DC-MBI, we found a first-order phase transition with a large hysteresis at high temperature; exothermic and endothermic peaks appeared at 369 and 399 K, respectively.

Discussion

The discovery of ferroelectricity provides firm evidence for proton tautomerism, which comprises proton transfer and concomitant π-bond switching. This intriguing issue has long been studied in both the solution and solid states and also addressed in relation to the large permittivity observed along the hydrogen-bonded chains of imidazole-related compounds. The ac electric fields employed for the permittivity measurements are a few orders of magnitude smaller than that required for polarization reversal and thus can probe only local fluctuations of the proton tautomerism and/or the bound motion of charged kink solitons on the hydrogen-bonded chains. As demonstrated for some benzimidazoles, this response may be tiny or even silent regardless of the ferroelectricity or antiferroelectricity especially when the Curie temperature is far above room temperature. In contrast, the reversal of a large polarization manifests collective switching that occurs in the whole crystal under a sufficiently large electric field. Incidentally, we note that in previous studies on the ferroelectricity of some imidazolium salts with inorganic anions, it was reported that the ferroelectricity arises from the orientational order–disorder phenomena of both dipolar component ions, whereas completely protonated imidazolium cations cannot trigger collective proton dynamics.

In addition to the chemical and thermal stability, the imidazole moieties have some advantages in terms of their substituent diversity. We found that the linear hydrogen-bonded chains can be aligned in various three-dimensional architectures. This feature is quite promising for finding new paradigms with various structure-property relationships, for instance, such as crystal symmetry and dimensionality. Polarity switching over two dimensions as seen for MBI is significantly advantageous for improving the polarization performance of the randomly orientated polycrystalline state, such as the thin-film form, compared with the uniaxial polarity available in other organic ferroelectrics except TEMPO (tanane). The observation of both ferroelectricity and antiferroelectricity in the imidazole sequence can be related to the minute energy difference between their polar and antipolar arrangements. These findings recall the excellent electromechanical response in some piezoelectric lead zirconate titanate (PZT) systems achieved by the electric-field-induced antiferroelectric to ferroelectric phase transition. It should also be noted that many imidazole-related compounds with various substituents are available from commercial sources and well-established chemical synthesis, and ferroelectric MBI is sold at low prices.

References

[1] S. Horiuchi, F. Kagawa, K. Hatahara, K. Kobayashi, R. Kumai, Y. Murakami, and Y. Tokura, Nature Commun. **3**, 1308 (2012).